

Article

Spreading Behavior and Morphology of Ethylene Methacrylic Acid (EMAA) Deposits via the Flame Spray Process

Wei Xie *, James Wang and Christopher C. Berndt

IRIS, Faculty of Engineering and Industrial Sciences, Swinburne University of Technology, PO Box 218, Hawthorn, VIC 3122, Australia; E-Mails: JAWang@groupwise.swin.edu.au (J.W.); CBerndt@groupwise.swin.edu.au (C.C.B.)

* Author to whom correspondence should be addressed; E-Mail: weixie@swin.edu.au; Tel.: +61-0-3-9214-5635; Fax: +61-0-3-9214-5050.

Received: 24 January 2012; in revised form: 6 April 2012 / Accepted: 22 May 2012 /

Published: 15 June 2012

Abstract: A single splat is the building block of a thermal spray coating; thus, investigating single splats is essential to understanding thermal spray coatings and their properties. In this study, the spreading behavior and the morphology of flame sprayed ethylene methacrylic acid (EMAA) splats, deposited at various stand-off distances (SODs) onto glass and mild steel substrates were investigated using optical microscopy, back scattered scanning electron microscopy and secondary electron scanning electron microscopy. The results of this study indicate that the spread factor increases with an increase in the stand-off distance up to 30 cm for glass and 25 cm for steel substrates. Further increase of the stand-off distance results in a decreased spread factor. The aspect ratio of EMAA single splats on both glass and mild steel substrates decreases with increased stand-off distances, indicating that more circular shapes occur at higher stand-off distances. On mild steel substrates, the minimum unevenness ratio (η) occurs at 35 cm SOD. The unevenness ratio (η) on glass substrates decreases from 1.9 (at 20 cm SOD) to 1.77 (at 25 cm SOD), and from 1.8 (at 30 cm SOD) to 1.3 (at 35 cm SOD). The lowest unevenness ratio (η) is found at 35 cm SOD. The highest unevenness ratio (η) is at 25 cm SOD. This paper discusses the effect of surface chemistry on the underside of an EMAA single splat morphology. It includes Raman spectrum analysis of EMAA and the X-ray diffraction of the EMAA powder. This work analyses the splat morphology and classifies the taxonomy of single splats of EMAA.

Keywords: thermal spray; single splat; EMAA; spread factor; aspect ratio

1. Introduction

Many parameters influence the structure of a single splat, and also, therefore, the thermal spray coating and its properties. The parameters are particle velocity; temperature; molten state; oxidation state; the substrate tilting angle; surface roughness; oxide layer composition and its thickness; and desorption of adsorbents and condensates. The physical properties of thermal conductivity and the wettability at impact between the thermal sprayed particle and the substrate influence the individual splat geometry [1,2] and the coating build-up and, consequently, the coating properties. The coating formation process is generally determined by the prime processing variables, which include substrate roughness, substrate temperature, impact velocity, stand-off distance (SOD), and the nature of the local atmospheric environment [3–6]. Many of these factors are inter-related. For example, SOD will influence the impact velocity as well as the substrate temperature due to heat transfer from the thermal spray torch.

The surface condition [7–10] and the wettability of the substrate plays an important role on the morphology of splats [11]. There are three factors affecting the wettability of the substrate. The first factor includes the substrate roughness, porosity and also the physical properties such as thermal conductivity. Higher surface roughness enhances wettability of the substrate [12], and higher thermal conductivity of the substrate, gives rise to poor wettability of the substrate [13]. The second factor includes the composition, thickness and morphology of the oxide layer on the surface of the substrate; these are affected by the preheating rate, temperature and time. The thickness of the oxide layer affects the roughness of the substrate [14], and thus modifies the wettability of the substrate [1]. The third factor concerns condensates or adsorbents on the substrate surface.

Wettability of the substrate is a factor that influences the maximum diameter of a single splat. Other factors include the droplet initial diameter, impact velocity, surface tension and viscosity. The wettability of the substrate plays a significant role when the impact velocity is low. The higher the wettability of the substrate, the greater the diameter of a single splat [15], and the less occurrence of a splash splat [16].

Single splat morphology is influenced by the critical preheating temperature T_c of the substrate [17]. The splats are more disc-like when the substrate temperature is over T_c . In contrast, the splats are extensively fingered when the temperature is below T_c . The value of T_c is relevant mainly to the splat material rather than the substrate [17].

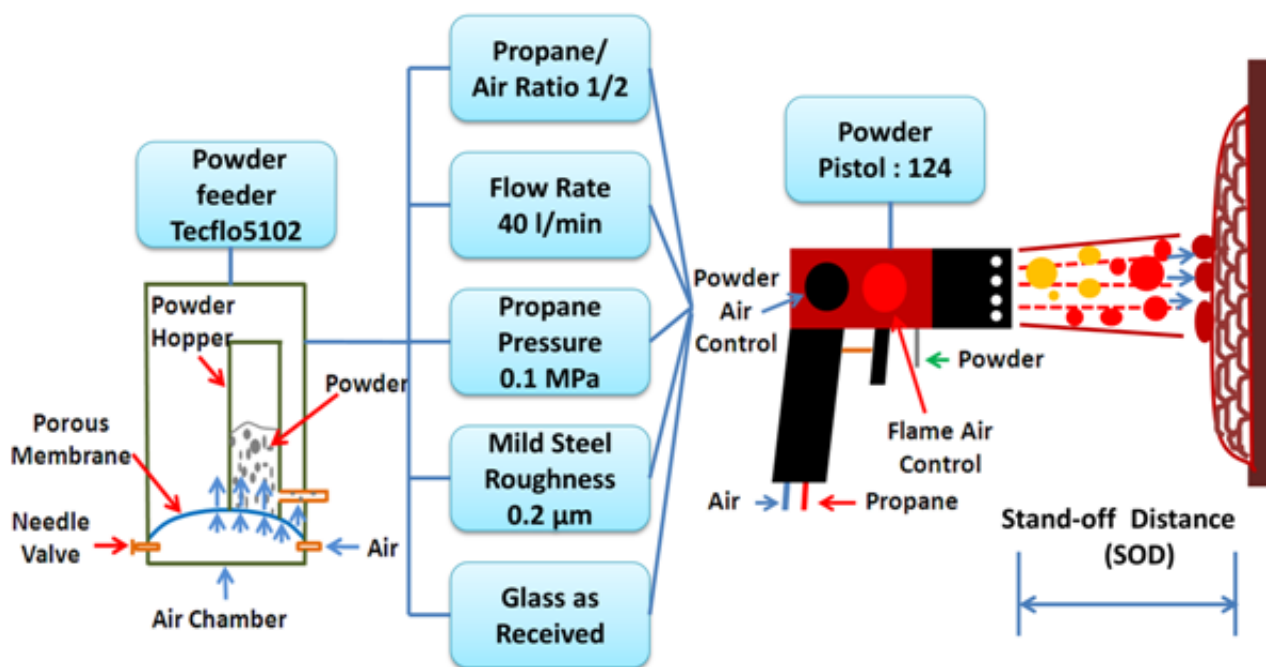
Many spray process parameters correlate to each other. The splat spread factor decreases with an increase in substrate roughness [18]. When the spray angle increases, splats exhibit an elliptical shape, and the aspect ratio; *i.e.*, the ratio of the length of the major axis to that of the minor axis of the splats, increases accordingly. The splats become fingered for spray angles less than 30° [17].

Spray process variables influence the physical nature of the intrinsic building blocks of thermal spray coatings; *i.e.*, the splat morphology [1,19]. The current work aims to investigate the effects of stand-off distance and the surface chemical condition on the splat spreading behavior and morphology.

2. Experimental Procedure

The spray process was performed with a Powder Pistol 124 PFS (Thermoplastic Powder Coatings, Big Spring, TX). The combustion gas was a propane/air mixture in the ratio of 1:2 at a flow rate of 40 L/min with the propane adjusted to 0.1 MP, see Figure 1. The maximum flame temperature is approximately 2,000 °C [20]. The flame velocity is about 50–100 ms⁻¹ [21].

Figure 1. Schematic of flame spray that indicates variables that are associated with the process.



A Tecflo 5102 fluidized bed powder feeder was used to spray single splats with propane (C₃H₈) as the fuel. The compressed air not only plays a role as an oxidant for the combustion process but also fluidizes the powder so that it can be delivered into the flame. The EMAA polymer particles are ejected through the flame and melted as droplets. The direction of droplet deposition was perpendicular to the substrate surface. The droplets then impinge on the substrate, deform and solidify, forming an interlaced network of splats. This work required single splats that did not overlap; therefore the powder flow rate was chosen to be much lower than flow rates typically used for forming a coating. Only one traverse with a traverse speed of 25 cm/s across the substrates without preheating (25 °C) was performed. The process parameters were selected according to thermal spray optimization. It can be argued that these processing conditions do not accurately represent industrial settings since typical industrial spray parameters would rule out the creation of non-overlapping splats. However, the authors wish to point out that the intent of the present study was to form single, individual splats for scientific observations.

EMAA, purchased from Innotek Powder Coatings, LLC, revealed a particle size from 30 μm to 400 μm (Figure 2) and exhibited an angular morphology (Figure 3), as expected because of the cryogenic grinding process used to manufacture the powders. The mean diameter of the particles was 140 μm and 85% particles were below 225 μm. The mode, or the most frequently occurring value [22],

of EMAA particles was 100 μm , and the particle size distribution was positively skewed. The properties of EMAA can be seen in Table 1.

Figure 2. Ethylene methacrylic acid (EMAA) particle size distribution.

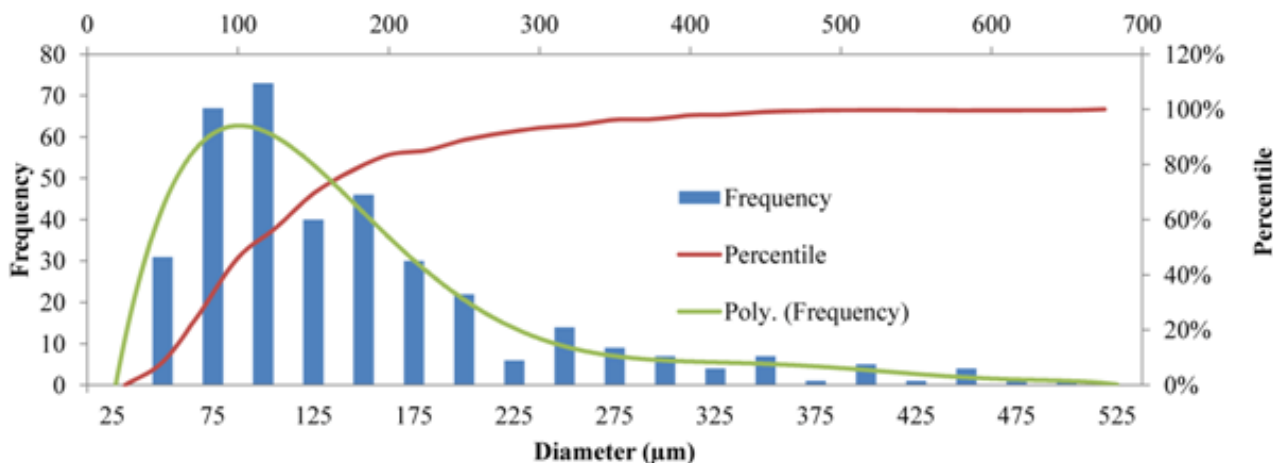
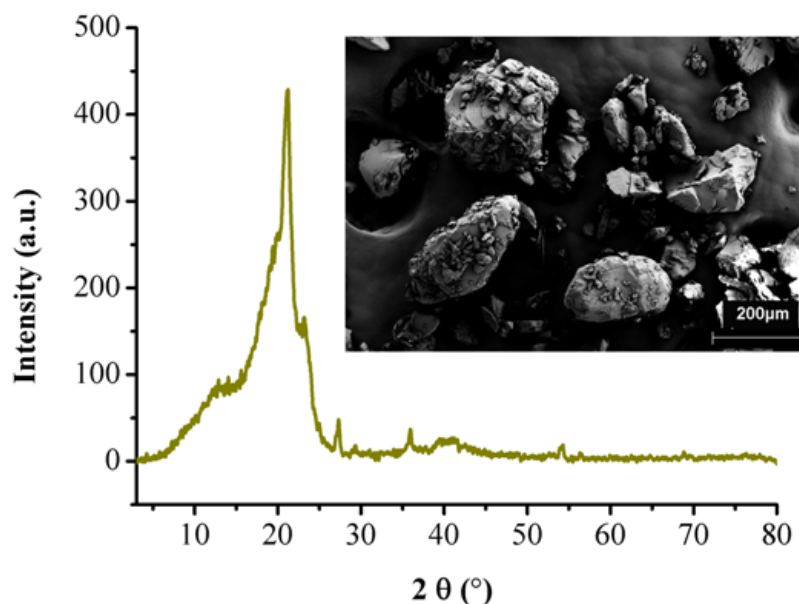


Figure 3. X-ray diffraction pattern of the EMAA powder and, inset, the morphology of EMAA powder.



The mild steel substrates of 20 mm \times 30 mm area and 2 mm thick were polished using silicon carbide sand paper and a diamond compound to achieve a 0.2 μm surface; whereas the glass slides were used in the as-received condition and were of average roughness 0.02 μm .

The sizes of particles and splats were measured using a Leica MEF4M optical microscope and image analysis software OLYSIA m3. The deposit morphology was examined through both secondary electron and backscattered electron images using scanning electron microscopy (ZEISS SUPRA 40VP FESEM). Samples were gold coated with a DYNAVAC CS 300 deposition system prior to the SEM analysis. The backscattered electron images provided an improved definition between polymer splats and the substrates [23]. The aspect ratio was analyzed with image analysis software ImageJ

(version 1.43) [24]. Each digital image under $50 \times$ magnification revealed 200 splats at 20 cm and 40 splats at 35 cm SOD. More than 400 splats were examined for each thermal spray condition.

Table 1. Properties of EMAA supplied by Innoteck (TD-Polyarmor G11 data sheet).

Property	Value
Melting Point	80–105 °C
Thermal Conductivity	0.33 $\text{wm}^{-1} \cdot \text{K}^{-1}$ [25]
Specific Gravity	>0.93
% Volatiles	negligible
Solubility in Water	negligible
Appearance and Odor	finely divided powder-mildly acidic odour
Color	grey
Flexibility (conical mandrel)	1/8 inch, no cracks (greater than 32%)
Adhesion	>1,000psi / (5A)
Impact Resistance	>384 in./lbs.
Gloss (at 60 degrees)	35–60
Hardness (Shore D)	48
Taber Abrasion	90 (mg loss, CS 10 wheel)* 100 (mg loss, CS 17 wheel)*
Dielectric Breakdown	893+/- 163 volts/mil**
Volume Resistivity	4.67 X 10 ¹³ Ohms/cm.
Salt Spray Resistance	>4,000 Hours
Humidity Resistance	No blistering or loss of gloss after 1,000 hours

* (1,000 g load/1,000 cycles). ** data obtained using 20 mil natural coatings. Addition of pigments may cause varying results.

The Raman spectrum of EMAA powder was performed with a Renishaw InVia Reflex Raman Spectrometer with an incident laser excitation wavelength at 785 nm and 514 nm. Spectra were collected and recorded within the range of 100–3,200 cm^{-1} at a spectrum resolution of 1 cm^{-1} . The splat profile, diameter, thickness and volume were analyzed with a VECCO WYKO NT1100 non-contact optical surface profilometer and its software (Vision V3.60).

3. Influence of Stand off Distance

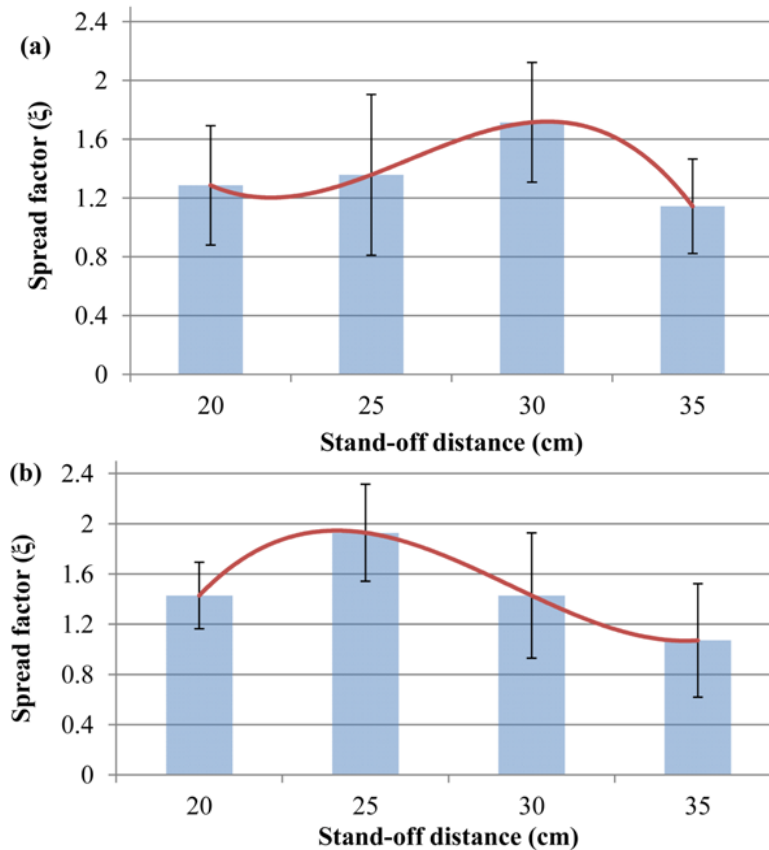
3.1. The Effect of Stand-off Distance on the Spread Factor of EMAA Single Splats

The spread factor, ξ , also known as the flattening ratio, is the ratio of the splat diameter, represented as an equivalent circle, to a droplet diameter [26]. The EMAA particle size is considered to be the original molten droplet diameter. Figure 4a indicates that the spread factor of splats on glass increased from 1.29 to 1.71 when the SOD increased from 20 cm to 30 cm, and decreased to 1.14 when the SOD increased to 35 cm. Figure 4b shows that the spread factor of splats on mild steel substrates increased from 1.43 to 1.93 when the SOD increased from 20 cm to 25 cm, and decreased to 1.07 at 35 cm SOD.

The maximum spread factor is achieved at a SOD of 30 cm and 25 cm, respectively, by depositing EMAA onto the glass and the mild steel substrates. A least squares cubic regression equation was used

to create the trend lines. Figure 4a demonstrates a negatively skewed curve, while Figure 4b exhibits a positively skewed curve.

Figure 4. The effect of stand-off distance on the spread factor of EMAA single splats on (a) Glass and (b) Mild steel substrates.



3.2. The Effect of Stand-off Distance on the Aspect Ratio of EMAA Single Splats

The aspect ratio, ψ , is the ratio of the length of the major axis to that of the minor axis of the ellipse, assuming that the splat is elliptical in shape [26]. Figure 5 demonstrates that the aspect ratio of EMAA decreased with an increase in the SOD, indicating an increase in circular splats with respect to the splashed splats. Figure 5a shows that the aspect ratio of EMAA on steel substrates is 1.47, 1.43, 1.31, 1.29 at 20, 25, 30, and 35 cm SOD, respectively; while the aspect ratio of EMAA on glass substrates, Figure 5b, is 1.41, 1.34, 1.27, 1.20 at 20, 25, 30, and 35 cm SOD, respectively.

The unevenness ratio (η) is the ratio of the border length of the flattened disc to the circumference of a circle [27], it can be expressed in the following Equation (1):

$$\eta = L/(2\pi R) \tag{1}$$

The term L is the boundary length of the irregular splat and R is the radius of a circle that has the same area as this splat. The degree of splashing (DS) is the ratio of the area of a splashed splat to that of a disc splat and is calculated according to Equation (2) [22]:

$$DS = \frac{1}{4\pi} \cdot \frac{L^2}{A} \tag{2}$$

In this alternative description of the splat, the term L is described as the perimeter of the splash and A is the area of the disc splat. When $DS = 1$, then the splat morphology is a perfect disc. The larger the DS , the more fingered or fragmented the splats. It can be shown that DS equivalent to η .

Figure 5. The effect of stand-off distance on the aspect ratio of EMAA single splats on (a) Glass and (b) Mild steel substrates.

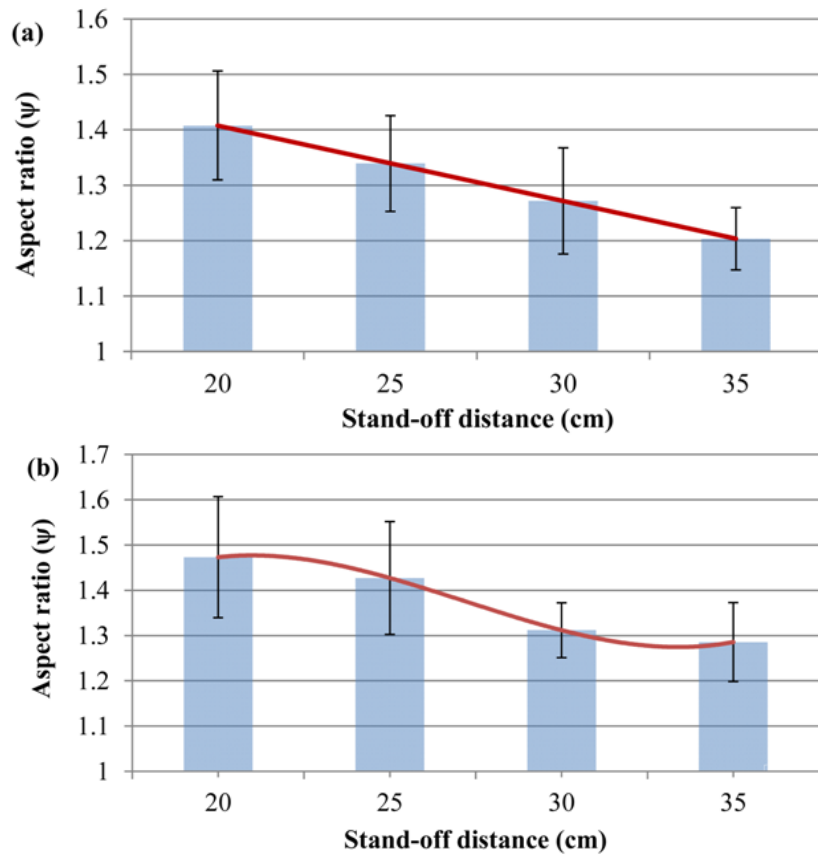


Figure 6. The effect of stand-off distance on the unevenness ratio of EMAA single splats (a) Glass and (b) Mild steel substrates.

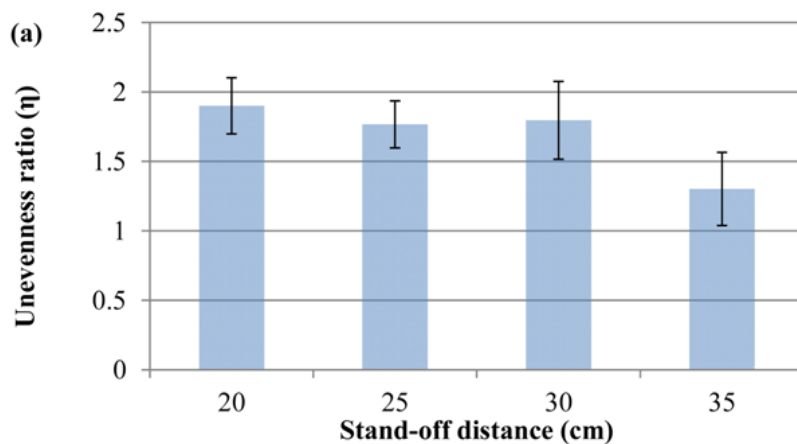
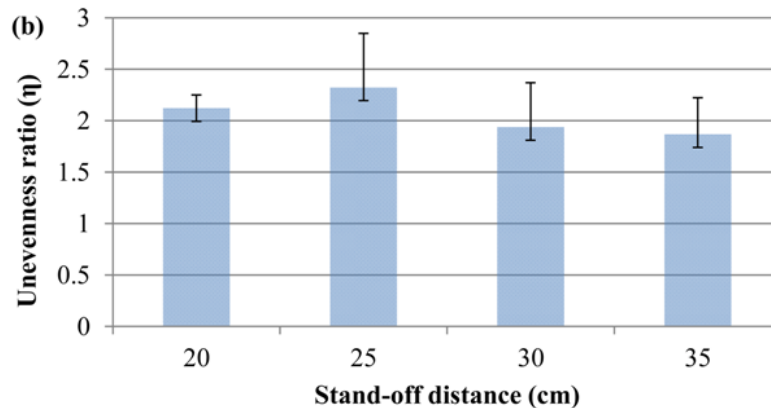


Figure 6. Cont.



The unevenness ratio (η) of all splat morphologies at 35 cm SOD could not be completely resolved using optical microscopy. The low flame temperature at a long stand-off distance resulted in the re-solidification of melted particles.

Figure 6 shows the variations of unevenness ratios (η) on glass and mild steel substrates. Generally the unevenness ratio (η) on glass substrates is smaller than that on mild steel substrates due to the lower thermal conductivity of glass in comparison to that of mild steel. The unevenness ratio (η) on glass substrates decreased from 1.9 (at 20 cm SOD) to 1.77 (at 25 cm SOD), and from 1.8 (at 30 cm SOD) to 1.3 (at 35 cm SOD). The lowest unevenness ratio (η) on glass was found at 35 cm SOD.

The unevenness ratio (η) on mild steel substrates increased from 2.12 (at 20 cm SOD) to 2.32 (at 25 cm SOD), and then decreased from 1.94 (at 30 cm SOD) to 1.87 (at 35 cm SOD). The minimum unevenness ratio (η) on mild steel occurred at 35 cm SOD and the highest unevenness ratio (η) arose at 25 cm SOD because the EMAA particles at 25 cm SOD exhibited a higher temperature and greater velocity.

4. Influence of Surface Chemistry

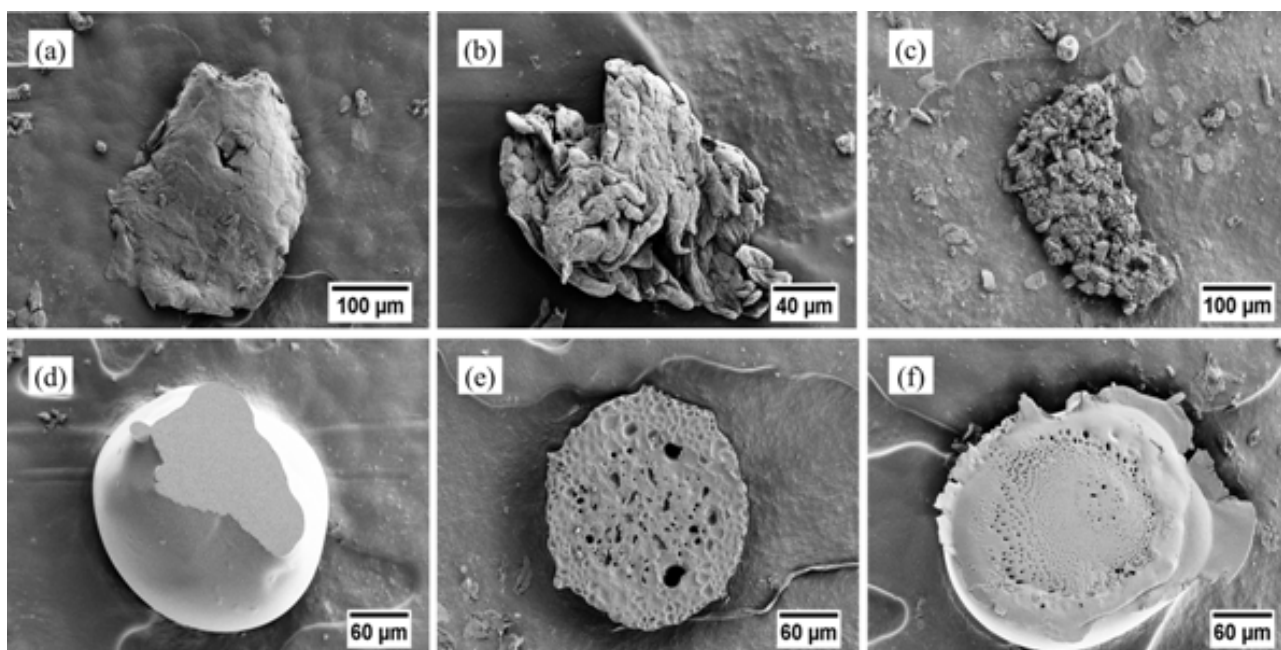
4.1. The Effect of Surface Chemistry on the Underside of EMAA Single Splat Morphology

The underside of EMAA single splat morphology is indicated in Figure 7. Unmelted particles are shown in Figure 7a and Figure 7b; while burnt particles are shown in Figure 7c. A single splat deposited onto a glass substrate is shown in Figure 7d and indicated that the bottom of the splat was smooth. The splats deposited on the surface of mild steel substrates at 25 cm and 35 cm SOD, Figure 7e and Figure 7f, reveal many “blow holes” on the bottom of both splats.

The blow holes arise from the volatility of condensates and adsorbates and have been described as arising from gas pockets, Jiang [7]. The amount and the size of the blow holes in Figure 7e are greater than those in Figure 7f due to the greater temperature of the melting droplet of EMAA in Figure 7e compared with Figure 7f. The trapped gas may result from (i) decomposition of EMAA under the spray conditions and/or (ii) gas release from the substrate due to input heat from the particle on impact, as studied by Tran [8,9] who researched aluminum and stainless steel substrates. It is deduced that mild steel would exhibit similar behavior since it is more readily oxidized and, therefore, has an enhanced ability to absorb condensates. However Fukumoto *et al.* [10] found that splat deposition on

gold substrates changed very little between “preheating” and “not preheating” conditions. In this case, the effect of surface chemistry on splat morphology was small because gold resists oxidation due to its noble character. It can be inferred that glass substrates should have the same effect, and that preheating the glass substrates will have little influence on the splat morphology.

Figure 7. The underside of EMAA single splat morphology (a) and (b) Unmelted particles. (c) Burnt particles. (d) A single splat deposited onto a glass substrate. (e) Splats deposited onto the surface of mild steel substrates at 25 cm stand-off distance. (f) Splats deposited on the surface of mild steel substrates at 35 cm stand-off distance.



4.2. Raman Spectrum Analysis of EMAA

The EMAA chemistry is shown in Figure 8 and was designated as “PF 113W” and procured from Plastic Flamecoat (Big Spring, TX). The melt index of 500 g/10 min corresponded to the lowest average molecular weight copolymer for EMAA. The EMAA has carboxyl groups (COOH) that which have the ability to ionize as represented by the following relationship; which is also a pH dependent phenomenon.

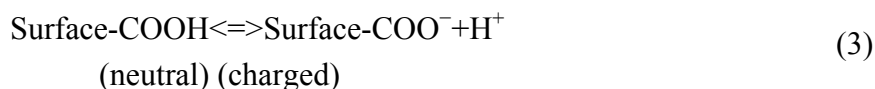


Figure 8. EMAA powder chemistry [20].

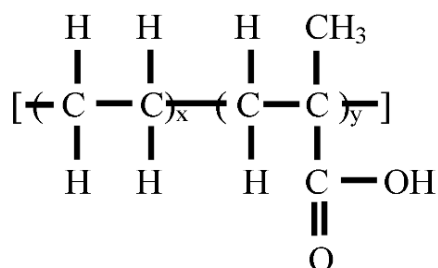
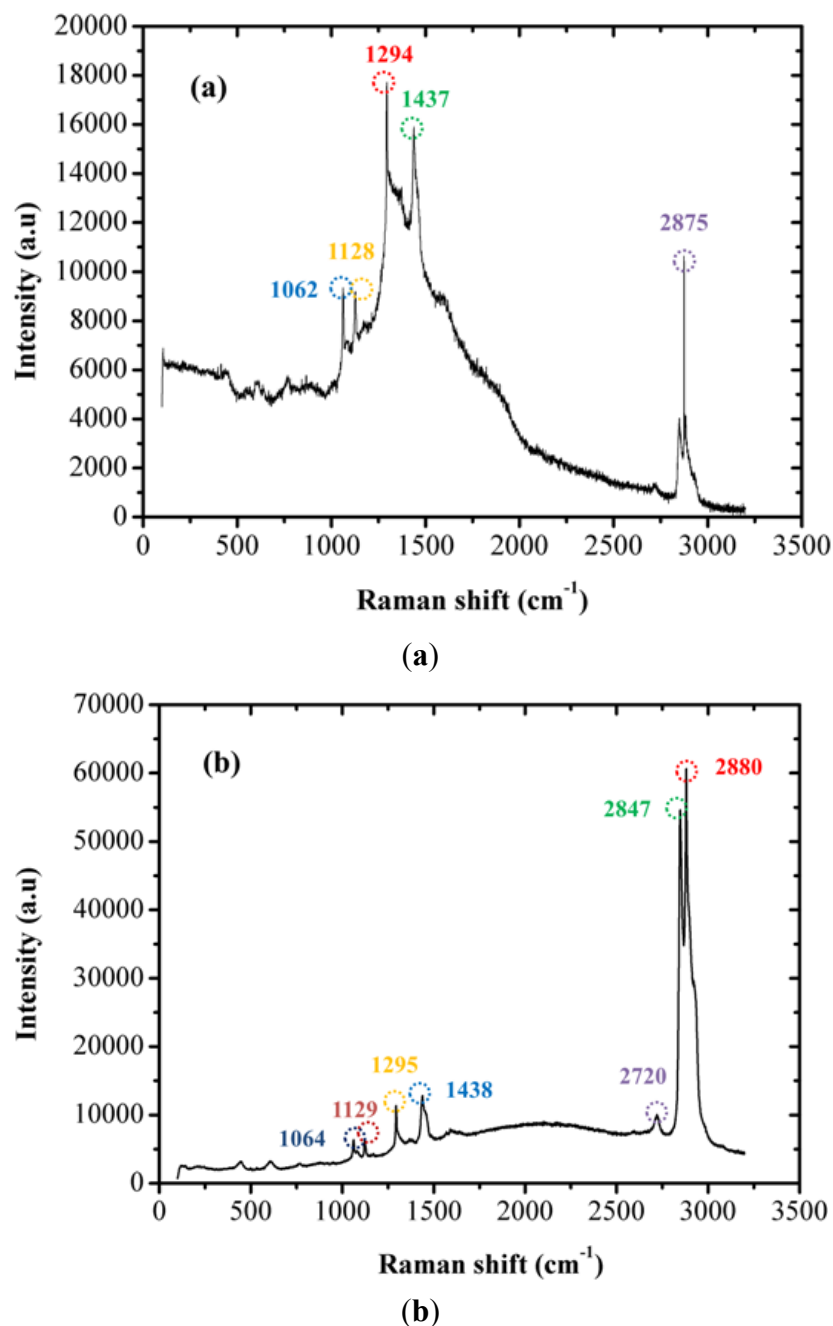


Figure 9. Raman spectrum of EMAA powder (a) Excitation wavelength at 785 nm; (b) Excitation wavelength at 514 nm.



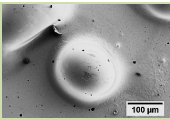
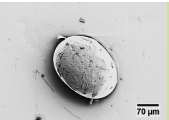
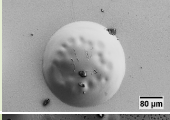
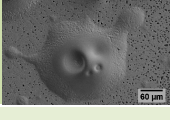
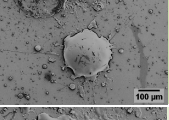
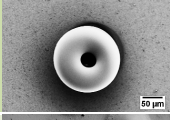
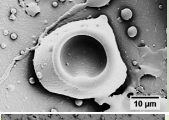
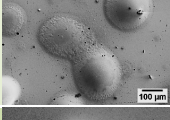
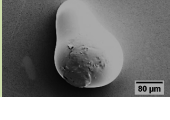
The Raman spectrum of EMAA is shown in Figure 9. The (C-H) group can be found in the band range of 2,874–2,880 cm⁻¹. The (CH₂) and (CH₃) asymmetric can be found in the band range of 2,874–2,880 cm⁻¹; whereas the (C-O-C) asymmetric occurs in the range of 1,062–1,129 cm⁻¹. The (C-C) alicyclic, aliphatic chain vibrations arise in the band range of 1,062–1,438 cm⁻¹. These function groups or vibrations fit well with EMAA chemical structure of (CH₂-CH₂)_x-(CH₂-CCH₃COOH)_y.

5. Taxonomic Analysis of Spats

5.1. Analysis of the Splat Morphology

Taxonomy is the science or technique of classification. From this research, the EMAA taxonomy can be classified into seven splat types, see Table 2. Spats can be classified as (i) semi-molten spats, (ii) disc spats, (iii) splashed spats, (iv) fragmented splashes, (v) doughnut spats, (vi) dumb bell spats, and (vii) re-solidified spats.

Table 2. Taxonomy of spats.

Taxonomy of spats	Glass		Mild steel	
Semi-melted spherical splat		<u>100 μm</u>		<u>70 μm</u>
Disc splat		<u>80 μm</u>		<u>80 μm</u>
Splashed splat		<u>60 μm</u>		<u>100 μm</u>
Splash fragment				<u>100 μm</u>
Doughnut splat		<u>50 μm</u>		<u>10 μm</u>
Dumbbell splat		<u>100 μm</u>		<u>100 μm</u>
Resolidified spherical splat		<u>80 μm</u>		<u>50 μm</u>

A splat refers to a pan cake shaped deposit, while a splash exhibits irregular and non-circular geometry with fingers and other features that may be connected or within the vicinity of a central mass of the coating material. An unmelted splat refers to particles that are partially melted and retain the near-spherical morphology of the feedstock material; whereas ‘re-solidified splat’ represents melted particles that have re-solidified and also maintain the near-spherical morphology of the feedstock material. Unmelted spats and re-solidified spats reflect a low processing temperature brought about by either short or long SODs, respectively. EMAA may not be melted completely during the short dwell time in the flame since it exhibits a low thermal conductivity of $0.33 \text{ Wm}^{-1} \cdot \text{K}^{-1}$ [25].

Figure 10 demonstrates the splat types created when sprayed at different distances onto two substrates. The delamination [28] or lift over [7] around the splat periphery was observed, Figure 10f, and arose from gas that escaped from the bottom of the splat. Figure 11 shows single spats deposited on glass substrates at SODs of (a) 20 cm, (b) 25 cm, (c) 30 cm and (d) 35 cm. Figure 12 shows typical

single splats deposited on mild steel substrates at SODs of (a) 20 cm, (b) 25 cm (c) at 30 cm. The morphology of the EMAA splats exhibit fragmentation when sprayed onto the mild steel substrates at room temperature, whereas a more regular, uniform disk was formed when sprayed onto glass substrates.

Figure 10. Type of splats (a) and (b) At 25 cm stand-off distance. (c) At 20 cm stand-off distance. (d) At 30 cm stand-off distance on glass substrates. (e), (f) and (g) At 20 cm stand-off distance on mild steel substrates.

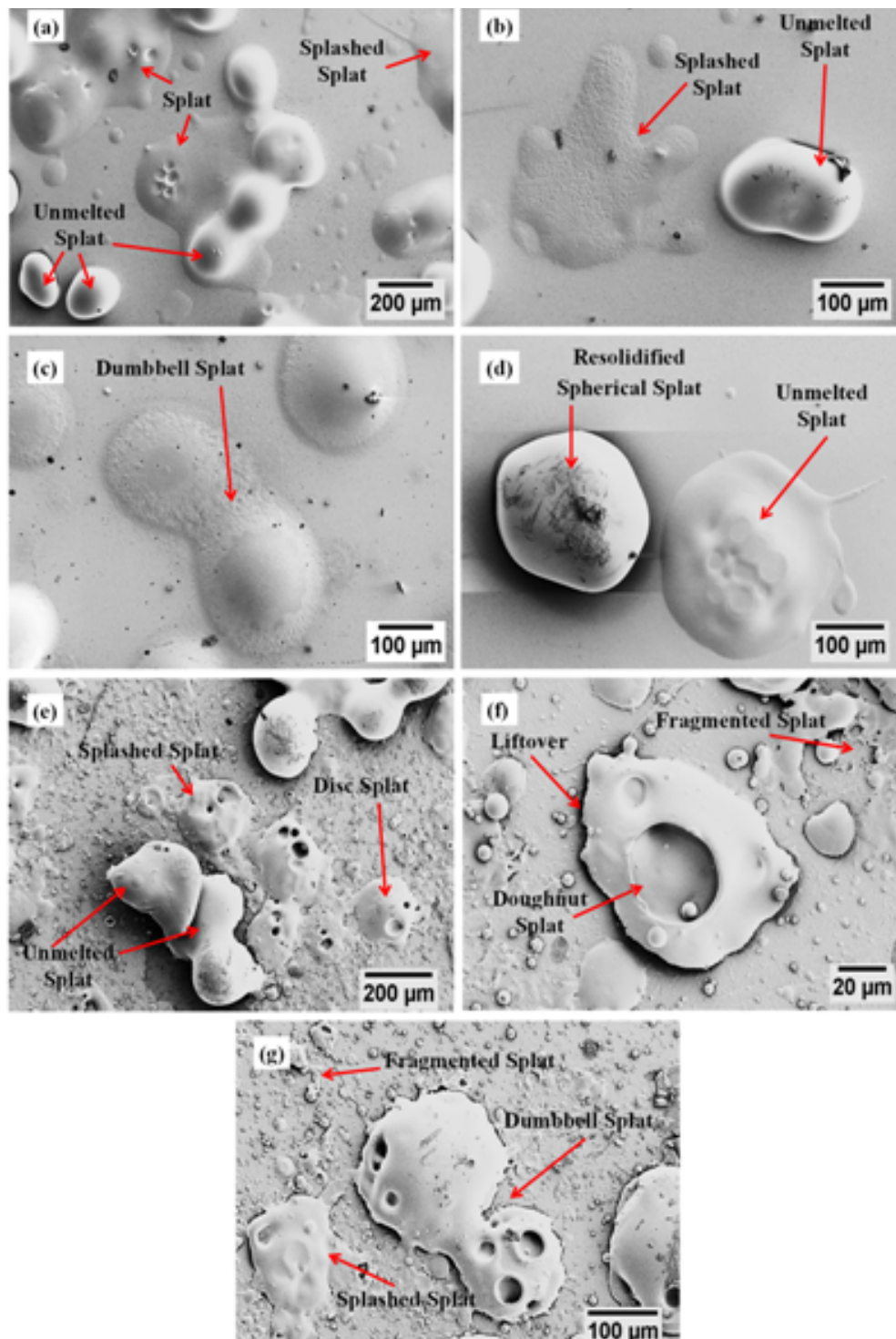


Figure 11. Typical single splats deposited on glass substrates (a) At 20 cm stand-off distance. (b) At 25 cm stand-off distance. (c) At 30 cm stand-off distance and (d) At 35 cm stand-off distance.

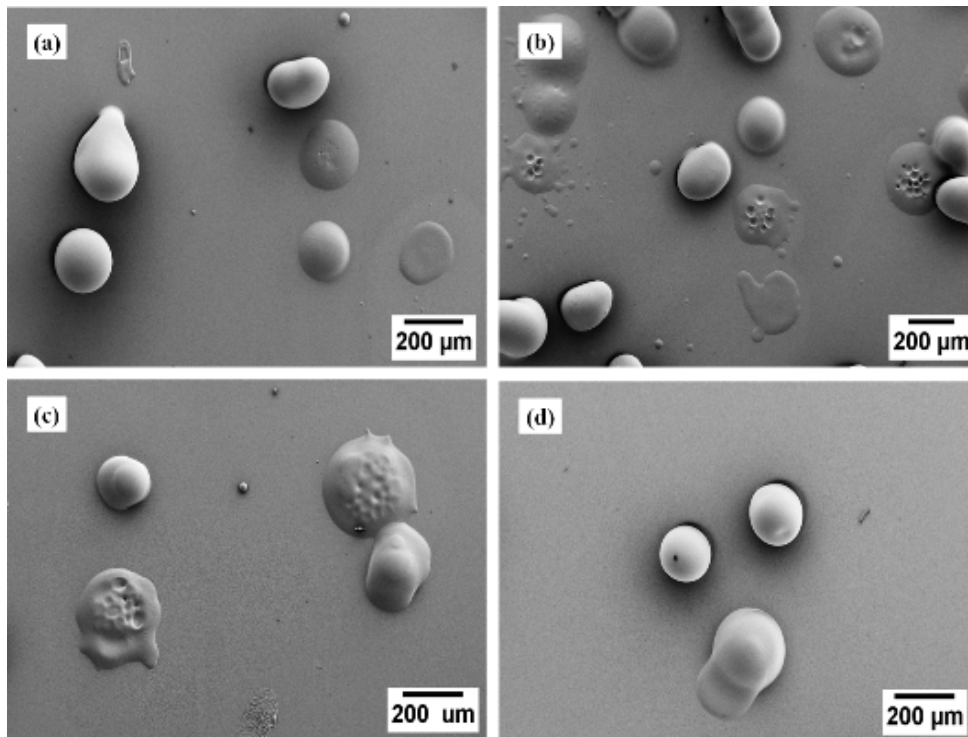
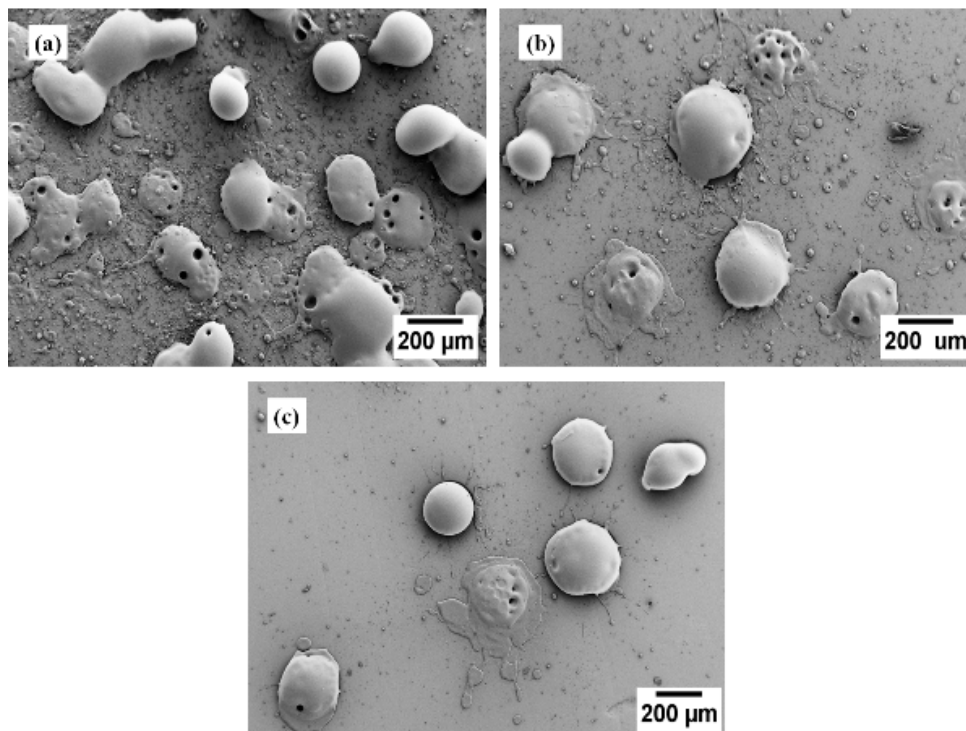


Figure 12. Typical single splats deposited on mild steel substrates (a) At 20 cm stand-off distance; (b) At 25 cm stand-off distance and (c) At 30 cm stand-off distance.



A higher percentage of a splash morphology was observed on mild steel substrates than glass substrates. It is suggested that more rapid freezing occurs on mild steel than on glass substrates due to

the higher thermal conductivity of the steel [29]. The thermal conductivity of the mild steel and glass substrates are $36\text{--}54 \text{ W}\cdot\text{m}^{-1}\cdot\text{K}^{-1}$ and $1.09\text{--}1.2 \text{ W}\cdot\text{m}^{-1}\cdot\text{K}^{-1}$ [30] respectively. Solidification of the splat when it makes first contact with the steel substrate impedes the liquid flow from the body of the molten drop and results in splashing. Therefore, in instances where splats are the preferred morphology then the mild steel substrate should be preheated [1,19,31]. Gas release from the substrate due to input heat from the particle at impact [8,32] is another mechanism that gives rise to splashing.

5.2. Surface Profile of Splat Morphology

The splashed splat and disk splat at 20 cm SOD on glass substrate were scanned using a WYKO surface profiler that is shown in Figure 13 and Figure 14 respectively. Figures 13a and 14a are the 3 dimensional images of splats; Figure 13b and 14b are top views of splat, while Figure 13c and 14c are splat cross sections. The physical measurements of the splashed splat are height = $7.6 \mu\text{m}$, diameter = $25 \mu\text{m}$, area = $4.647 \times 10^{-3} \text{ mm}^2$ and volume = $2.09 \times 10^4 \mu\text{m}^3$. The corresponding measurements of the disc splat are height = $7 \mu\text{m}$, diameter = $160 \mu\text{m}$, area = $69 \times 10^{-3} \text{ mm}^2$ and volume = $3.98 \times 10^5 \mu\text{m}^3$.

Figure 13. Splashed splat scanned by WYKO surface profiler (a) 3D display; (b) Top view; (c) Cross section of splat.

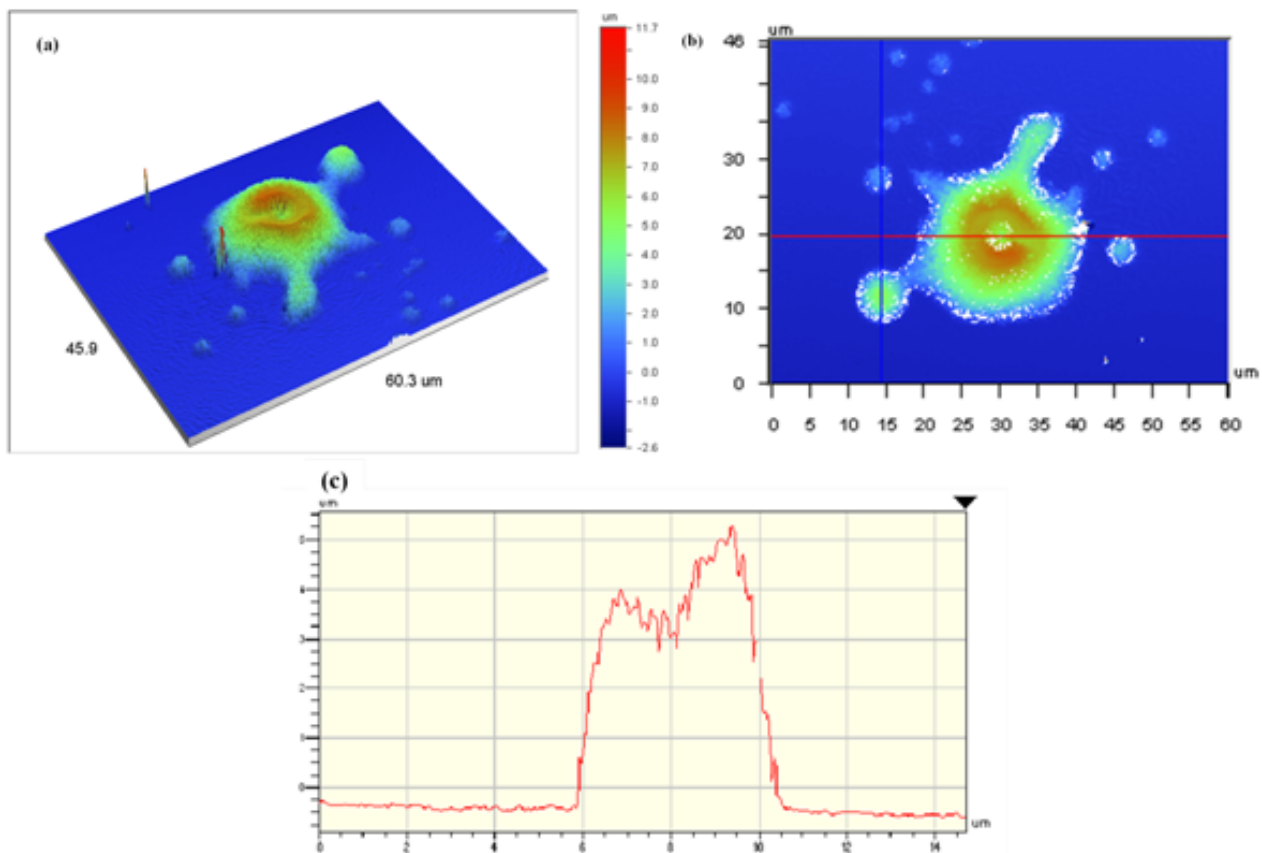
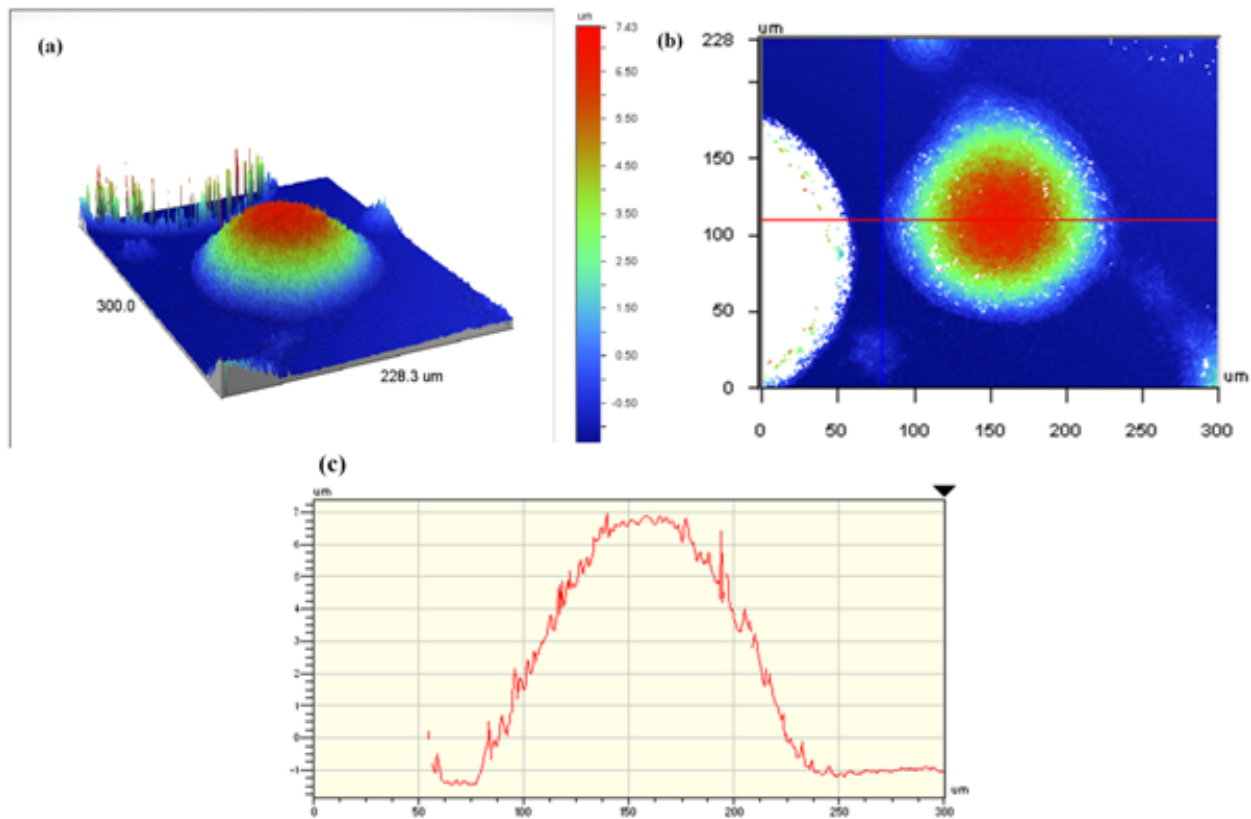


Figure 14. Disk splat scanned by WYKO surface profiler (a) 3D display; (b) Top view; (c) Cross section of splat.



6. Conclusions

The spread factor increases with an increase in the SOD until 30 cm and 25 cm for glass and steel substrates, respectively. Increasing the SOD above 30 cm on glass substrates and 30 cm on steel substrates results decreases the spread factor and decreases the aspect ratio of EMAA single splats on both glass and mild steel substrates decreased, which means more circular shapes occur at a higher SOD. On mild steel substrates, the minimum unevenness ratio (η) occurs at 35 cm SOD. The unevenness ratio (η) on glass substrates decreases from 1.9 (at 20 cm SOD) to 1.77 (at 25 cm SOD), and from 1.8 (at 30 cm SOD) to 1.3 (at 35 cm SOD). The lowest unevenness ratio (η) is found at 35 cm SOD. The highest unevenness ratio (η) is at 25 cm SOD.

The surface chemistry of the substrates plays a crucial role on splat morphology. The volatiles of condensates introduce bubbles to the splats, produce splashed splats and even fragmented splats. The Raman spectra of EMAA power and single splat demonstrate that there is no degradation of EMAA during the flame spray process. The taxonomy of single splats researched in this paper has concluded that there are seven types of single splats: (i) semi-molten splats and (ii) re-solidified splats, (iii) disc splats, (iv) fingered splashes, (v) fragmented splashes, (VI) doughnut splats and (VII) dumbbell splats. This study provides practical guidance about the nature of how prime spray variables influence processing/morphology relationships.

Acknowledgments

The Thermal Spray Group at Swinburne University of Technology has supported this work. Dr. Stoddard and Dr. White assisted with the Raman instrument and analysis. Dr. Malherbe helped with the XRD experiments. Professor Nick (Monash University) provided access to the WYKO surface profiler. Mr. Wei Xie is the recipient of a Swinburne University Postgraduate Research Award (SUPRA).

References

1. Fauchais, P.; Fukumoto, M.; Vardelle, A.; Vardelle, M. Knowledge concerning splat formation: An invited review. *J. Therm. Spray Technol.* **2004**, *13*, 337–360.
2. Verdian, M.M.; Salehi, M.; Raeissi, K. Effect of feedstock particle size on microstructure of APS coatings prepared from mechanically alloyed nickel-titanium powders. *Surf. Eng.* **2010**, *26*, 447–452.
3. Sweet, G.K. Applying Thermoplastic/Thermoset Powder with a Modified Plasma System. In *Proceedings of the 1993 National Thermal Spray Conference*, Anaheim, CA, USA, 7–11 June 1993; Berndt, C.C., Ed.; ASM International: Materials Park, OH, USA, 1993; pp. 381–384.
4. Vardelle, A.; Moreau, C.; Fauchais, P. The dynamics of deposit formation in thermal-spray processes. *MRS Bull.* **2000**, *25*, 32–37.
5. Bussmann, M.; Chandra, S.; Mostaghimi, J. Modeling the splash of a droplet impacting a solid surface. *Phys. Fluids* **2000**, *12*, 3121–3132.
6. Herman, H.; Sampath, S.; McCune, R. Thermal spray: Current status and future trends. *MRS Bull.* **2000**, *25*, 17–25.
7. Jiang, X.; Wan, Y.; Herman, H.; Sampath, S. Role of condensates and adsorbates on substrate surface on fragmentation of impinging molten droplets during thermal spray. *Thin Solid Films* **2001**, *385*, 132–141.
8. Tran, A.T.T.; Hyland, M.M.; Qiu, T.; Withy, B.; James, B.J. Effects of surface chemistry on splat formation during plasma spraying. *J. Therm. Spray Technol.* **2008**, *17*, 637–645.
9. Tran, A.T.T.; Hyland, M.M.; Shinoda, K.; Sampath, S. Influence of substrate surface conditions on the deposition and spreading of molten droplets. *Thin Solid Films* **2011**, *519*, 2445–2456.
10. Fukumoto, M.; Nagai, H.; Yasui, T. Influence of surface character change of substrate due to heating on flattening behavior of thermal sprayed particles. *J. Therm. Spray Technol.* **2006**, *15*, 759–764.
11. Zhao, B.; Yadian, B.L.; Li, Z.J.; Liu, P.; Zhang, Y.F. Improvement on wettability between carbon nanotubes and Sn. *Surf. Eng.* **2009**, *25*, 31–35.
12. Fukumoto, M.; Nishioka, E.; Matsubara, T. Effect of interface wetting on flattening of freely fallen metal droplet onto flat substrate surface. *J. Therm. Spray Technol.* **2002**, *11*, 69–74.
13. Tanaka, Y.; Fukumoto, M. Investigation of dominating factors on flattening behavior of plasma sprayed ceramic particles. *Surf. Coat. Technol.* **1999**, *120–121*, 124–130.

14. Christoulis, D.K.; Pantelis, D.I.; Borit, F.; Guipont, V.; Jeandin, M. Effect of Substrate Roughness and Temperature on splat Formation in Plasma Sprayed Aluminium Bronze. In *Proceedings of the 18th International Conference on Surface Modification Technologies*, Dijon, France, 15–17 November 2004; ASM International: Materials Park, OH, USA, 2006; pp. 73–83.
15. Li, R.; Ashgriz, N.; Chandra, S. Maximum spread of droplet on solid surface: Low Reynolds and Weber numbers. *J. Fluids Eng. Trans. ASME* **2010**, *132*, doi:10.1115/1.4001695.
16. Fukumoto, M.; Huang, Y. Flattening mechanism in thermal sprayed nickel particle impinging on flat substrate surface. *J. Therm. Spray Technol.* **1999**, *8*, 427–432.
17. Fauchais, P.; Vardelle, A.; Dussoubs, B. Quo vadis thermal spraying? *J. Therm. Spray Technol.* **2001**, *10*, 44–66.
18. Leger, A.C.; Vardelle, M.; Vardelle, A.; Dussoubs, B.; Fauchais, P. Splat formation: Ceramic particles on ceramic substrates. In *Proceedings of the 8th National Thermal Spray Conference*, Houston, TX, USA, 11–15 September 1995; Bernd, C.C.; Sampath, S. Eds; ASM International: Materials Park, OH, USA, 1995; pp. 169–174.
19. Sampath, S.; Jiang, X.Y.; Matejicek, J.; Leger, A.C.; Vardelle, A. Substrate temperature effects on splat formation, microstructure development and properties of plasma sprayed coatings part I: Case study for partially stabilized zirconia. *Mater. Sci. Eng. A* **1999**, *272*, 181–188.
20. Brogan, J.A.; Berndt, C.C. The coalescence of combustion-sprayed ethylene-methacrylic acid copolymer. *J. Mater. Sci.* **1997**, *32*, 2099–2106.
21. Petrovicova, E.; Schadler, L.S. Thermal spraying of polymers. *Int. Mater. Rev.* **2002**, *47*, 169–190.
22. Lin, C.-K. Statistical Approaches to Study Variations in Thermal Spray Coatings Variations in Thermal Spray Coatings. Ph.D. Dissertation, State University of New York, Stony Brook, NY, USA, 1995.
23. Withy, B.P.; Hyland, M.M.; James, B.J. The effect of surface chemistry and morphology on the properties of hvaf peek single splats. *J. Therm. Spray Technol.* **2008**, *17*, 631–636.
24. Rasband, W.S. *ImageJ*; U.S. National Institutes of Health: Bethesda, MD, USA, 1997–2010.
25. Brogan, J.A. Processing and Property Relationships of Thermally Sprayed Polymer Systems. Ph.D. Dissertation, State University of New York, Stony Brook, NY, USA, 1996.
26. Kang, C.W.; Ng, H.W. Splat morphology and spreading behavior due to oblique impact of droplets onto substrates in plasma spray coating process. *Surf. Coat. Technol.* **2006**, *200*, 5462–5477.
27. Amada, S.; Tomoyasu, K.; Haruyama, M. Splat formation of molten Sn, Cu and Ni droplets. *Surface and Coatings Technology* **1997**, *96*, 176–183.
28. Tran, A.T.T.; Hyland, M.M. The role of substrate surface chemistry on splat formation during plasma spray deposition by experiments and simulations. *J. Therm. Spray Technol.* **2010**, *19*, 11–23.
29. Jiang, X.; Matejicek, J.; Sampath, S. Substrate temperature effects on the splat formation, microstructure development and properties of plasma sprayed coatings part II: Case study for molybdenum. *Mater. Sci. Eng. A Struct. Mater. Prop. Microstruct. Process.* **1999**, *272*, 189–198.
30. Nishioka, A.; Nishio, M.; Koda, T.; Ikeda, S.; Koyama, K. The effects of metal cation types on zero shear viscosities for ethylene-co-methacrylic ionomer melts. *Nihon Reoroji Gakkaishi* **2005**, *33*, 199–204.
31. Bianchi, L.; Grimaud, A.; Blein, F.; Lucchese, P.; Fauchais, P. Comparison of plasma-sprayed alumina coatings by rf and dc plasma spraying. *J. Therm. Spray Technol.* **1995**, *4*, 59–66.

32. Nishioka, A.; Koda, T.; Miyata, K.; Murasawa, G.; Koyama, K. The effects of small contents of water on melt rheology for ethylene-methacrylic zinc ionomers. *Polym. J.* **2008**, *40*, 350–353.

© 2012 by the authors; licensee MDPI, Basel, Switzerland. This article is an open access article distributed under the terms and conditions of the Creative Commons Attribution license (<http://creativecommons.org/licenses/by/3.0/>).